JOURNAL of
MATERIALS and MECHATRONICS:A

e-ISSN 2717-8811
JournalMM, 2024, 5(1), 87-105
https://doi.org/10.55546/jmm.1451429

## Araştırma Makalesi / Research Article

# Large Deflection Analysis of Functionally Graded Beam by Using Combining Method

Ersin DEMİR[1*], Hasan ÇALLIOĞLU[2], Zekeriya GİRGİN[3]

[1*] Pamukkale University, Faculty of Technology, Department of Mechatronics Engineering, Denizli, Turkey,
ORCID ID: https://orcid.org/0000-0001-8222-5358, edemir@pau.edu.tr
[2] Pamukkale University, Faculty of Technology, Department of Mechatronics Engineering, Denizli, Turkey,
ORCID ID: https://orcid.org/0000-0002-4598-7975, hcallioglu@pau.edu.tr
[3] Pamukkale University, Faculty of Engineering, Department of Mechanical Engineering, Denizli, Turkey
ORCID ID: https://orcid.org/0000-0001-5958-9735, (Retired)

**Geliş/ Received:** 12.03.2024**;** **Revize/Revised:** 20.04.2024 **Kabul / Accepted:** 08.05.2024

**ABSTRACT:** In this study, the large deflection behavior of a circular cross-section beam is examined using the Combining Method (CM). The CM is a numerical solution method that uses block diagrams in the Matlab-Simulink program and weighting coefficients in the Differential Quadrature Method (DQM). The beam material considered is Functionally Graded Material (FGM). Boundary conditions of the beam are taken as clamped-free (C-F) and a singular load is assumed to be applied from the free end of the beam. Geometric nonlinear analysis is performed while calculating the large deflection equations of the beam and performing numerical analysis. The effects of increasing the force applied to the beam, changing the beam cross-section in the longitudinal direction, and changing the material index of the FGM on the extreme deflection behavior of the beam were examined. For comparison purposes, the results obtained from CM are compared with the results obtained from both SolidWorks-Simulation and Ansys-Workbench programs. As a result of the analysis, increasing the applied force causes the x and y coordinates of the end point of the beam to decrease. The change in geometry and material index greatly affects the large deflection occurring in the beam.

**Keywords:** Large Deflection, Functionally Graded Material, Beam, Combining Method, Finite Element Method

## 1. INTRODUCTION

Beams are widely used in many fields of engineering applications (mechanical, civil, etc.). Therefore, the behavior of beam structures (deflection, vibration, buckling, etc.) has been studied intensively by many researchers. When studying the deflection behavior of beams, simplifications are made based on certain assumptions due to the non-linearity of the governing equation representing

*Sorumlu yazar / Corresponding author: edemir@pau.edu.tr
Bu makaleye atıf yapmak için /To cite this article

Demir, E., Çallıoğlu, H., Girgin, Z. (2024). Large Deflection Analysis of Functionally Graded Beam by Using Combining Method. Journal of Materials and Mechatronics: A (JournalMM), 5(1), 87-105.

the deflection behavior of the beam. In recent years, especially with the development of numerical analysis techniques, the default simplifications have been removed to make more accurate analysis. Therefore, the problem of large deflection of beams has attracted the attention of many researchers. For example, Belendez et al. (2002) examined the large deflection behavior of a cantilever beam under a singular load from its free end. In their study, they expressed the nonlinear governing equation that represents the system. They solved the governing equation theoretically and compared it with the experimental results. Dado and Al-Sadder (2005) studied the large deflection behavior of prismatic and non-prismatic cantilever beams under different loads. The nonlinear governing equation they established has been solved theoretically for the problem considered. They also compared their results with the results obtained from the Msc/Nastran program.

Another issue addressed in this study is FGM. The concept of FGM was first proposed in 1984 in Japan by Japanese scientists during thermal barrier research conducted for a spacecraft (Koizumi, 1993). The use of FGM materials is advantageous because the material properties of the mentioned structure can be modified as desired from one surface to another. Below, some of the articles in the open literature examining the large deflection behavior of beams made of FGM are summarized.

Kang and Li (2010) studied the large deflection of a cantilever beam made of FGM. It is assumed that a moment is applied from the free end of the beam under consideration. They derived the explicit expression of the beam considered in their study. As a result, they determined the optimum gradient distribution for FGM and suggested the appropriate beam design. Davoodinik and Rahimi (2011) studied the large deflection of a FG beam. The beam is assumed to be flexible, with a tapered cross-section. It is also assumed that the considered beam is subjected to inclined end loading and intermediate loading. As a result of using the semi-analytical method, the effects of the taper ratio, inclined end loading, and material distribution on the large deflection behavior were examined. Brojan et al. (2012) studied the large deflections of thin non-prismatic beams under non-uniform distributed load and concentrated load acting from the free end. The material of the beam is assumed to be a nonlinear elastic material. They compared the theoretical results obtained with experimental results and existing results in the literature. Soleimani (2012) derived the large deflection equation of a beam consisted of FGM under arbitrary load. In the study, it is assumed that the elasticity modulus of the beam varies with the exponential and power function in the longitudinal direction of the beam. Shooting Method was used for analysis. As a result of the analysis, the effect of using different elasticity modulus functions and applying different loadings on the large deflection behavior of the beam was examined. Kien (2013) examined the large deflection behavior of a cantilever beam made of axial FGM with a tapered cross-section. In the study, the effects of inhomogeneity of the beam material, shear deformation, and non-uniform section on the large deflection behavior of the beam were investigated. Sitar et al. (2014) studied the solution of the differential equation obtained for the large deflection behavior of a thin inhomogeneous beam. It is assumed that the beam consists of thin layers throughout the thickness. In this way, it was desired to obtain an FG beam whose material properties change continuously throughout the thickness. They solved the derived equations numerically and compared them with the existing results in the literature. Horibe and Mori (2018) solved the equation for the large deflection behavior of a thin tapered beam made of FGM. A transverse load is applied to the free end of the beam. They used the Runga-Kutta method in their solutions. They compared the deflection and bending stress results obtained as a result of their solutions with the existing results. Lin et al. (2019) overcame the large deflection problem of the axial FG beam with the Homotopy Analysis Method. It is assumed that the beam is cantilever and the load

is applied from its free end. Moreover, it is assumed that the elasticity modulus varies along the beam length. They compared their results with the results obtained from the finite element method and previous studies. Saraçoğlu et. al. (2019) calculated the deflections of orthotropic beams using Euler-Bernoulli and Timoshenko beam theories. In their study, orientation angle, material properties, and length/depth ratio were examined in the static analysis of orthotropic beams. Saraçoğlu et. al. (2022) studied equal strength cantilever and simply supported beams made of functionally graded material under uniformly distributed load or point load. Dimensionless deflections of the beams considered were obtained for different material indices. Nguyen et. al. (2022a) studied the large deflection behavior of a two-phase FG sandwich beam with different homogeneity. They used a nonlinear finite element method in their study. In their study, they used four types of homogenization methods to obtain the effective elastic modulus of the beam. In the study, the Newton-Rapson Method and Arc-Length technique were used to find the large deflection and stress distribution of the beam. Nguyen et al. (2022b) developed a model based on Isogeometric analysis for the large deflection of curved FG beams. They also used a 3-dimension beam theory in their study. They considered five benchmark test cases to demonstrate the accuracy of their proposed solution technique. Additionally, the effect of material variations on curved beam behavior under different loads is also expressed. Li et al. (2022) proposed a non-local numerical model for large deformation analysis of variable cross-section FG beam. They used the peridynamic differential operator in the solution of their study. They also used variational analysis, the Lagrange multiplier method, and the Newton-Rapson method to solve the governing equation. They applied their proposed method to the large deflection analysis of a homogeneous cantilever beam and a linearly and parabolically varying cantilever FG beam. They also compared their results with finite element results.

With the development of technology in the last twenty years, computer processor speeds have increased considerably. Thus, the interest in numerical techniques has constantly increased accordingly. Numerical techniques attract the attention of scientists in solving problems that cannot be easily solved with theoretical calculations. CM, one of these numerical techniques, was first proposed by Girgin (2008) for the solution of nonlinear differential equations. Girgin stated in his study that the conditions cannot be applied at any instant in the time domain while making solutions in computer-aided numerical programs. He stated that this problem could be overcome by combining Matlab/Simulink, one of the computer-aided numerical programs, and the DQM, another numerical technique. Thus, the shortcomings of DQM, which cannot be easily used in solving nonlinear problems, and the shortcomings of Matlab/Simulink in applying boundary conditions have been eliminated. After this study, Girgin (2009) applied the same technique to the Integral Quadrature Method (IQM). Thus, derivative and integral operations in nonlinear equations with boundary conditions can be easily performed. Moreover, Girgin et al. (2014) applied CM to four different nonlinear differential equations. These equations have not only initial conditions but also boundary conditions. They compared the results obtained from CM with the results available in the literature. In addition, Girgin et al. (2020) carried out a large deflection analysis of the prismatic embedded beam for different loading conditions. Unlike this study, the material is isotropic and the beam cross-section is taken as constant. Additionally, the iterative DQM method was also proposed in this study.

Furthermore, there are a few studies in which only DQ methods are used when performing large deflection analyses of beams. Kurtaran (2015) examined the large deflection of moderately thickness FG curved beams for static and transient behavior using the generalized DQM. He expressed the spatial derivatives in the equilibrium equation with generalized DQM. He solved the static

equilibrium equation using the Newton method and the dynamic equilibrium equation using the Newmark method. Hu et al. (2017) formulated the nonlinear large deflection contact problem for curved beams. They proposed a new adaptive DQ element method to predict the contact positions in the curved beam. Demir (2023) solved the problem of large displacement behavior of a Functionally Graded beam under uniform thermal load. He examined the effects of temperature, material, geometry, slenderness, force, and boundary conditions on the large displacement of the beam.

In this study, the large deflection behavior of a cantilever beam with a variable cross-section made of FGM is studied. CM method is used to solve the complex nonlinear governing differential equation. In addition, the results obtained with CM were compared with the results obtained from Ansys-Workbench and SolidWorks-Simulation programs for comparison purposes. Since the problem addressed in the literature research has strong non-linearity, the studies generally require the application of complex calculation procedures. However, the complex nonlinear differential equation mentioned with CM can be easily solved. As a result of comparison with the results obtained from finite element-based programs, it is seen that quite compatible values are obtained.

## 2. GEOMETRIC AND MATERIAL PROPERTIES OF THE BEAM

### 2.1 Geometry

The geometry of the FG beam is shown in Fig. 1. It can be seen from the figure that the boundary condition of the beam is C-F and the cross-section of the beam is a variable that depends on the variable r(s) along the longitudinal direction. ro is the radius of the beam at the clamped end.

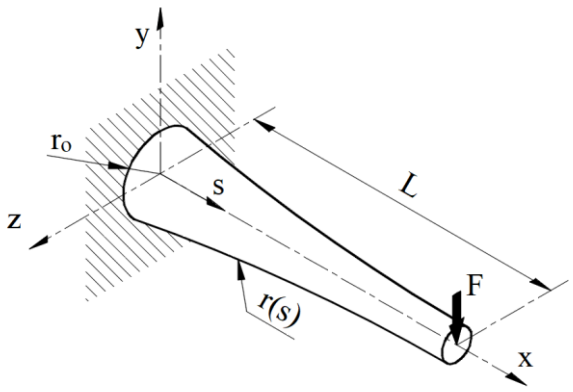


**Figure 1.** The FG beam with variable cross-section

The force (*F*) is applied at the free end of the beam. *L* is the length of the beam. *x*, *y* and *z* refers to the coordinates in the longitudinal, transverse, and normal direction and *s* is the curvilinear coordinate of the beam along the deflection direction. The radius of the beam varies along the *s* coordinate and is given by the formula in Eq. 1.

$$r(s) = r_o\left(1 + \left(\frac{s}{L}\right)\right)^{n1} \tag{1}$$

where *n1* is a geometric index. In this study, *n1* is taken as -0.3, -0.15, 0, 0.15 and 0.3. $r_o$ and *L* are taken as 10 and 1000 mm, respectively. So, the variation of *r(s)* depending on the geometric index is obtained as shown in the Figure 2. As can be seen from the figure, the cross-section of the beam is constant when *n1*=0.

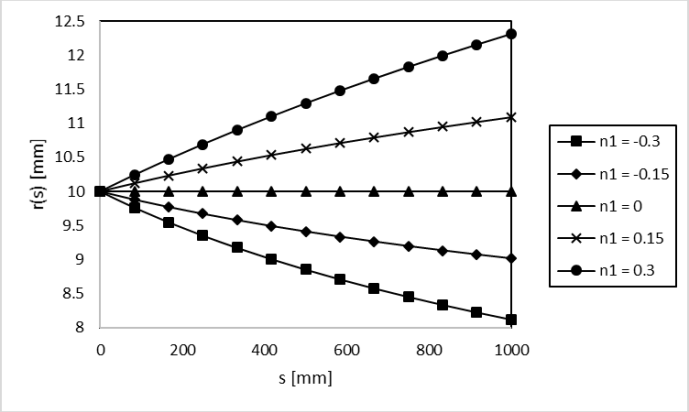


**Figure 2.** Variation of the radius of the beam with *s* coordinate

Additionally, it can be seen from the figure that the cross-section increases when the *n1* value is positive and decreases when it is negative.

### 2.2 Material

It is assumed that the material of the beam is functionally graded material. The properties of the beam material are varied from the clamped end to the free end. That is, similar to the change in radius, the material properties of the beam also vary along the s coordinate. This variation is given for the Elasticity Modulus in the Eq. 2.

$$E(s) = E_o\left(1 + \left(\frac{s}{L}\right)\right)^{n2} \tag{2}$$

where *n2* is a material index. *n2* is taken as -0.7, -0.4, 0, 0.4 and 0.7. $E_o$ is the Elasticity Modulus of the beam at the clamped end. In this study, the material at the clamped end is taken as Aluminum and its Elasticity modulus is 70000 N/mm$^2$. The variation in the elasticity modulus (*E(s)*) depending on the material index is obtained as shown in the Fig. 3.

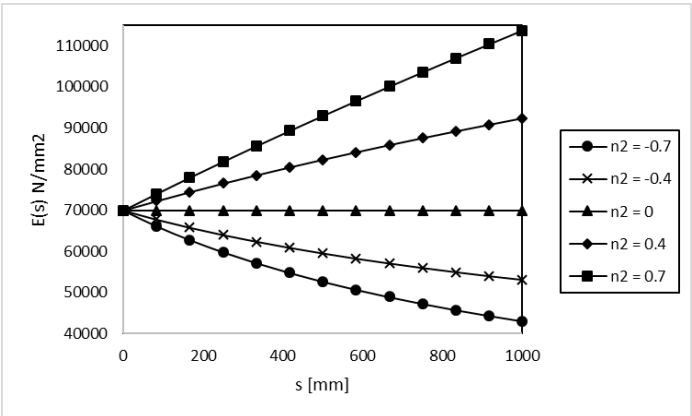


**Figure 3.** Variation in the Elasticity modulus of the beam with *s* coordinate

As can be seen from the figure, the Elasticity modulus of the beam is constant when *n2*=0 and it increases when the *n2* value is positive and it decreases when *n2* is negative.

## 3. THEORETICAL FORMULATION OF THE BEAM

The large deflection behavior of a functionally graded beam with variable cross-section is considered in this study. The variable cross-section beam with a singular load applied from its free end is shown on the left in Fig. 4 (Dado and Al-Sadder, 2005).

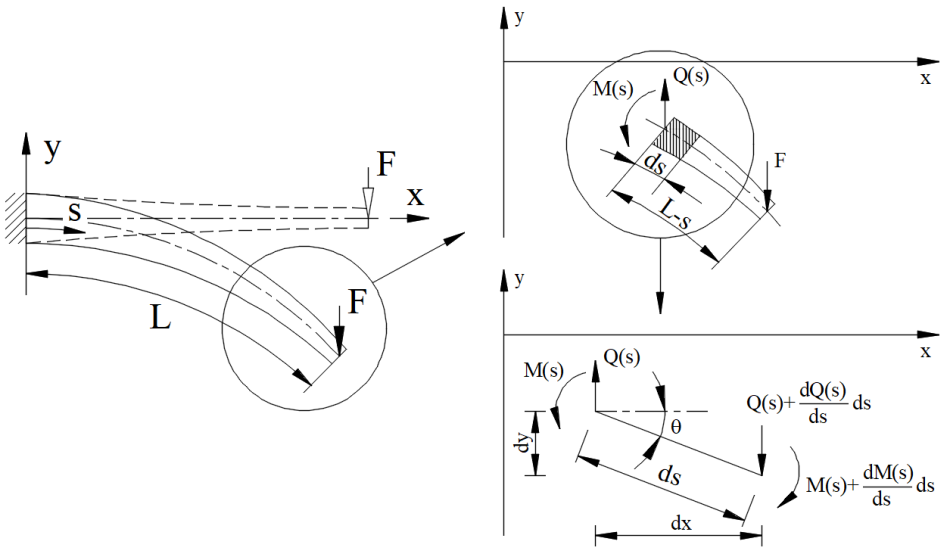


**Figure 4.** Variation in the Elasticity modulus of the beam with *s* coordinate

The free-body diagram of the free-end section of the considered beam is shown in the upper right of Fig. 4. When the force equilibrium in the vertical direction is written here, the following equation is obtained.

$$Q(s) = F \tag{3}$$

Here Q(s) and F are the internal and external vertical forces, respectively. In the bottom right corner of Fig. 4, a free-body diagram is shown by considering the infinitesimal element of the beam section under consideration. If the moment equilibrium is written in the infinitesimal element, it yields:

$$\frac{dM(s)}{ds} ds + Q(s)\, dx = 0 \tag{4}$$

When both sides of the equation are divided by ds, it gives,

$$\frac{dM(s)}{ds} + Q(s)\, \frac{dx}{ds} = 0 \tag{5}$$

The following equations can be obtained from the figure showing the infinitesimal element.

$$\frac{dy}{ds} = sin\theta \tag{6}$$

$$\frac{dx}{ds} = cos\theta \tag{7}$$

where θ is the slope of the beam.

When Eq. 7 is substituted into Eq. 5, the following equation yields.

$$\frac{dM(s)}{ds} = -Q(s)\,cos\theta \tag{8}$$

When Eq. 3 is substituted into Eq. 8, it gives,

$$\frac{dM(s)}{ds} = -F\,cos\theta \tag{9}$$

In addition, according to the Euler–Bernoulli law, the following equation can be written.

$$M(s) = E(s)I(s)\frac{d\theta}{ds} \tag{10}$$

*E(s)* in Eq. 10 was given in Eq. 2. *I(s)* is the variable area moment of inertia of the beam and, it is given in Eq. 11.

$$I(s) = \pi\frac{\left(r(s)\right)^4}{4} \tag{11}$$

*r(s)* in Eq. 11 was given in Eq. 1. The derivative of Eq. 10 with respect to *ds* is given in Eq. 12.

$$\frac{dM(s)}{ds} = \left(\frac{dE(s)}{ds}I(s) + E(s)\frac{dI(s)}{ds}\right)\frac{d\theta}{ds} + E(s)I(s)\frac{d^2\theta}{ds^2} \tag{12}$$

When this resulting equation is substituted in Eq. 9, the following governing equation can be obtained as similar to Reference (Dado and Al-Sadder, 2005).

$$\left(\frac{dE(s)}{ds}I(s) + E(s)\frac{dI(s)}{ds}\right)\frac{d\theta}{ds} + E(s)I(s)\frac{d^2\theta}{ds^2} + F\,cos\theta = 0 \tag{13}$$

When Eqs. 1 and 2 are substituted in Eq. 13, the following general equation is obtained,

$$\frac{d\theta}{ds} = \frac{1}{(n2+4n1)}\left(-\frac{d^2\theta}{ds^2}(L+s) - \frac{4(L+s)\,F\,cos\theta}{E_o\,\pi r_o^4}\left(\frac{L+s}{L}\right)^{-n2}\left(\frac{L+s}{L}\right)^{-4n1}\right) \tag{14}$$

The nonlinear differential equation obtained is normalized for the solution with CM. For this, the expression *s* is made dimensionless as follows,

$$s = S\,L \tag{15}$$

where S is normalized form of s.

Thus, the following normalized equation is obtained. This equation is used to solve the problem.

$$\frac{d\theta}{dS} = \frac{1}{(n2+4n1)}\left(-\frac{d^2\theta}{dS^2}(1+S) - \frac{4L^2(S+1)\,F\,cos\theta}{E_o\,\pi r_o^4}(1+S)^{-n2}(1+S)^{-4n1}\right) \tag{16}$$

The C-F boundary conditions of the beam are given in Eqs. 17-20.

$$y(0) = 0 \tag{17}$$

$$x(0) = 0 \tag{18}$$

$$\theta(0) = 0 \tag{19}$$

$$\left.\frac{d\theta(s)}{ds}\right|_{s=L} = 0 \tag{20}$$

## 4. THE SOLUTION WITH COMBINING METHOD

The CM used in this study is implemented in the Simulation module of the Matlab program. While CM is applied, the weight coefficients obtained for the derivatives and integrals in DQM are used for the derivative and integration operations needed to solve the nonlinear differential equation. The procedure for obtaining weight coefficients for derivative and integral are explained in Sections 4.1 and 4.2.

### 4.1 Weighting Coefficients for Derivatives

The first-order derivative of a function *f(x)* is given in DQM as follows (Girgin,2008),

$$\frac{df(x_i)}{dx} = \sum_{j=1}^{N} A_{ij}^{(1)} f(x_i) \qquad (i = 1,2,\dots,N) \tag{21}$$

where $A_{ij}^{(1)}$ is the weighting coefficients of the first-order derivative of the function *f(x)*. The test functions are obtained from the following Lagrange interpolation shape functions.

$$l_i(x) = \frac{\Phi(x)}{(x - x_i)\Phi^{(1)}(x_i)} \qquad (i = 1,2,\dots,N) \tag{22}$$

where

$$\Phi(x) = \prod_{i=1}^{N}(x - x_i) \tag{23}$$

$$\Phi^{(1)}(x_i) = \frac{d\Phi(x_i)}{dx} = \prod_{j=1, j\neq i}^{N}(x_i - x_j) \tag{24}$$

By substituting Eq. 22 into Eq. 21, weighting coefficients for first-order derivatives are obtained as follows.

$$A_{ij}^{(1)} = \frac{dl_j(x_i)}{dx} = \frac{\Phi^{(i)}(x_i)}{(x_i - x_j)\Phi^{(1)}(x_j)} \qquad (i,j = 1,2,\dots,N), \qquad i \neq j \tag{25}$$

$$A_{ii}^{(1)} = \frac{dl_i(x_i)}{dx} = -\sum_{j=1, i\neq j}^{N} A_{ij}^{(1)} \qquad (i = 1,2,\dots,N) \tag{26}$$

These obtained coefficients are the elements of the weighting coefficients matrix of the first-degree derivative $[A^{(1)}]$. The coefficients of higher-order derivatives are calculated with the following formula,

$$[A^{(r)}] = \frac{d^r}{dx^r} = \frac{d}{dx}\frac{d^{r-1}}{dx^{r-1}} = [A^{(1)}][A^{(r-1)}] \tag{27}$$

In this study, widely used equally spaced sampling points are selected in normalized coordinates as given in Eq. 28,

$$x_i = \frac{i-1}{N-1} \qquad (i = 1,2,\dots,N) \tag{28}$$

**4.2 Weighting Coefficients for Integrals**

Integral coefficients and integral constant coefficients are used to obtain the function itself from its first-order derivative (Girgin, 2009).

$$\int \frac{df(x_i)}{dx}dx = \sum_{j=1}^{N} B_{ij}^{(1)} \frac{df(x_i)}{dx} + \sum_{j=1}^{N} C_{ij}^{(0)} f(x_i) \qquad (i = 1,2,\dots,N) \tag{29}$$

where $B_{ij}^{(1)}$ and $C_{ij}^{(0)}$ are weighting coefficients of the single integral and coefficients of the integral constant, respectively. The following process is applied to find $B_{ij}^{(1)}$ weight coefficients

$$D_{ij} = \frac{x_i - g}{x_j - g} A_{ij}^{(1)} \quad i \neq j \quad (i,j = 1,2,\dots,N) \tag{30}$$

$$D_{ii} = A_{ii}^{(1)} + \frac{1}{x_i - g} \quad i = j \quad (i,j = 1,2,\dots,N) \tag{31}$$

where $A_{ij}^{(1)}$ is the weighting coefficients of the first-order derivative and $g$ is constant and is not equal to $x_i$. If the inverse of matrix $[D]$ is taken as matrix $[H]$, the elements of matrix $[B]$ are obtained from the elements of matrix $[H]$ as follows:

$$B_{ij}^{(1)} = H_{ij} - H_{1j} \qquad (i,j = 1,2,\dots,N) \tag{32}$$

As for the coefficients of the integral constant $C_{ij}^{(0)}$, they are given in Eq. 33.

$$C_{ij}^{(0)} = \begin{cases} 1 & for \quad j = 1 \\ 0 & for \quad j \neq 1 \end{cases} \qquad (i, j = 1,2, \dots, N) \tag{33}$$

### 4.3 Solution

The normalized governing differential equation (Eq. 16) is integrated to find the θ rotation function in the solution of the problem under consideration. To make the solution more understandable with CM, complex expressions are embedded into subsystems as shown in Eq. 34.

$$\theta = \int \left( \underbrace{\frac{1}{(n2 + 4n1)}}_{Subsystem\ A} \left( -\frac{d^2\theta}{dS^2} \underbrace{(1+S)}_{Subsystem\ B} - \underbrace{\frac{4L^2(S+1)\,F}{E_o\ \pi r_o^4}}_{Subsystem\ C} cos\theta \underbrace{(1+S)^{-n2}}_{Subsystem\ D} \underbrace{(1+S)^{-4n1}}_{Subsystem\ E} \right) \right) dS \tag{34}$$

Eq. 34 can be written briefly as Eq. 35,

$$\theta = \int \left( A \left( -\frac{d^2\theta}{dS^2}\ B - \ C\ cos\theta\ D\ \ E \right) \right) dS \tag{35}$$

After finding the θ value in Eq. 35, x and y values at each point of the beam are obtained from Eqs. 6 and 7 as Eqs. 36 and 37, respectively.

$$y = \underbrace{\int sin\theta\, dS}_{Subsystem\ F} \tag{36}$$

$$x = \underbrace{\int cos\theta\ dS}_{Subsystem\ G} \tag{37}$$

While solving a differential equation with Matlab/Simulink, the blocks in the library are brought to the work area by drag and drop method and combined to define the equation. Although it is very easy to define the initial conditions in solving the differential equation with Matlab/Simulink, the boundary conditions needed in the differential equation expressing the beam problem cannot be entered. Therefore, this problem was overcome by combining this method with the DQM. Fig. 5 shows the design of Eqs. 34, 36, and 37 using CM in the Matlab/Simulink environment.

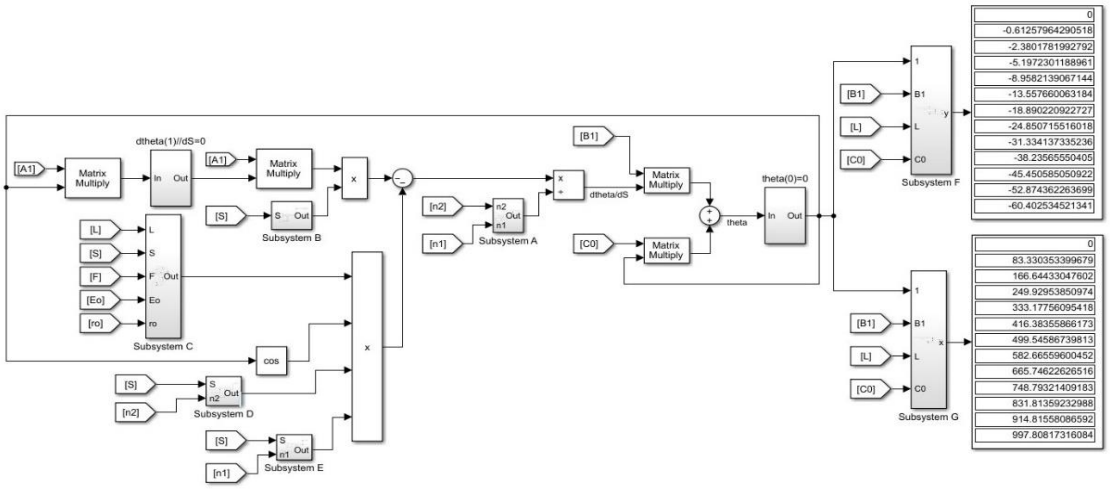


**Figure 5.** Block diagram of Eqs. 34, 36 and 37

First of all, the four operations in Eq. 34 are performed by combining the necessary blocks (sum, subtract, etc.), and the integral and derivative operations are performed using the weight coefficients in DQM. The operations in Eqs. 36 and 37 are shown on the right side of the main block diagram. The constants and weighting coefficients shown in Fig. 5 are also defined as shown in Fig. 6.

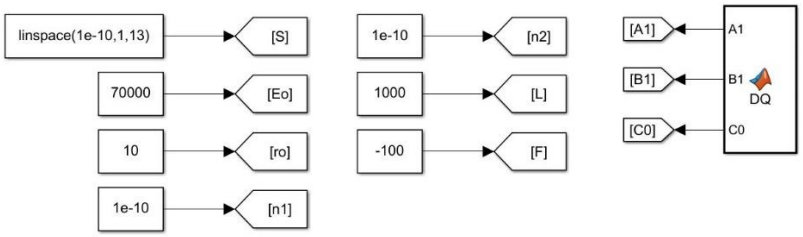


**Figure 6.** Constants and weighting coefficients in the previous figure

The weighting coefficients expressed in Sections 4.1 and 4.2 are defined in the DQ block shown in Fig. 6. As seen in the figure, the S value is normalized and taken within the range [0,1]. It is assumed that there are 13 sampling points in the beam. In addition, the subsystems shown in Fig. 5 are given in Figs. 7-13, respectively.

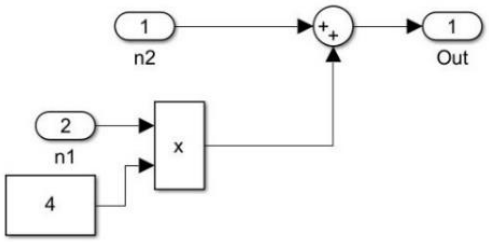


**Figure 7.** Block diagram of Subsystem A

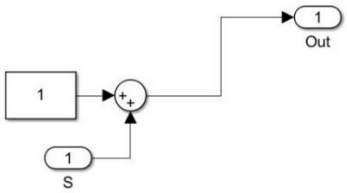


**Figure 8.** Block diagram of Subsystem B

Subsystems A and B given in Eq. 34 are shown in Figs. 7 and 8. Subsystem A is the denominator of the fractional expression. The other subsystems C, D, E, F, and G are shown in Figs. 9-13, respectively.

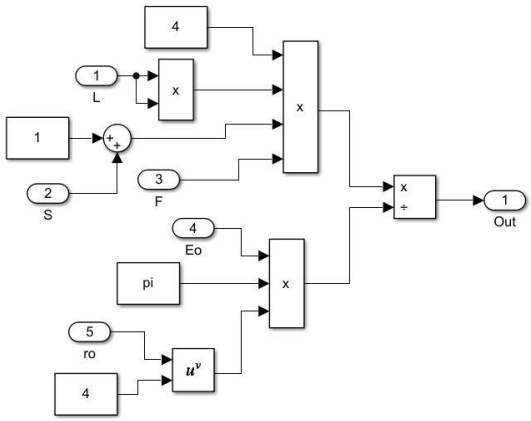


**Figure 9.** Block diagram of Subsystem C

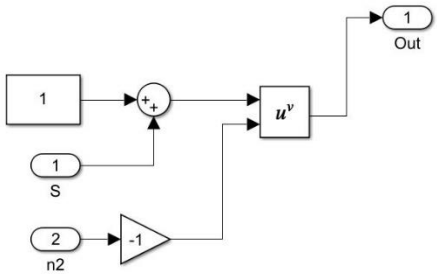


**Figure 10.** Block diagram of Subsystem D

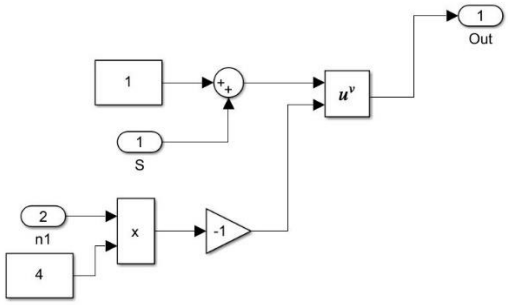


**Figure 11.** Block diagram of Subsystem E

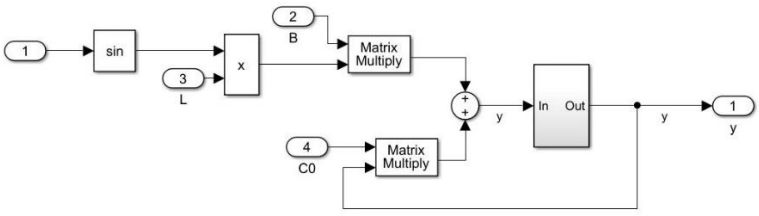


**Figure 12.** Block diagram of Subsystem F

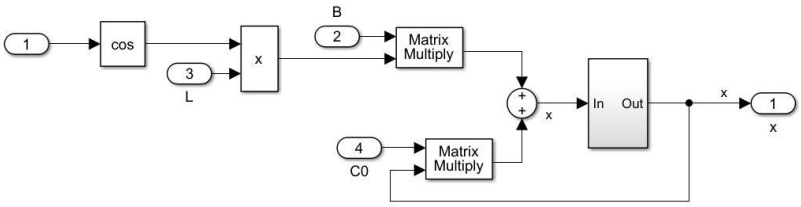


**Figure 13.** Block diagram of Subsystem G

Additionally, the subsystems where boundary conditions are entered, as seen in the main block diagram, are provided in Fig. 14.

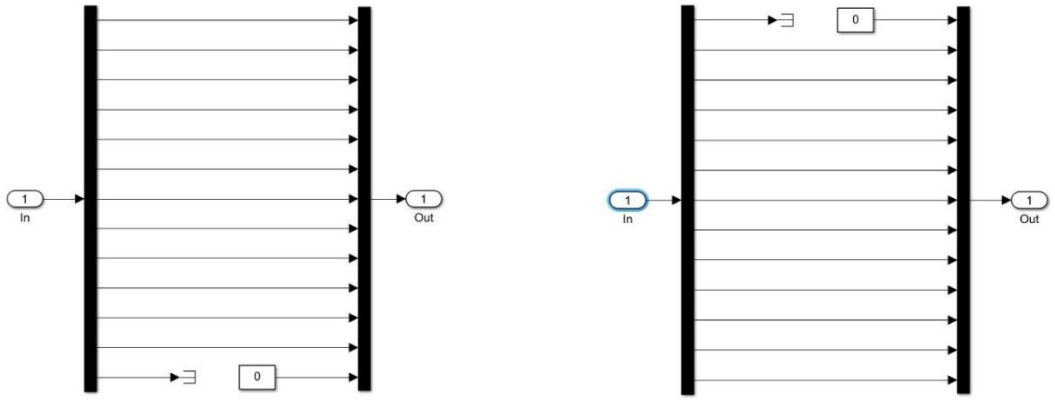


**(a)** $\frac{d\theta(1)}{ds} = 0$ **(b)** $\theta(0) = 0$

**Figure 14.** Block diagrams of boundary conditions.

As mentioned above, assuming that there are 13 sampling points in the beam, the incoming signal has been divided into 13 branches and later merged. The boundary condition is entered from the relevant sampling point.

## 5. FINITE ELEMENT-BASED SOLUTION

In order to verify the results obtained with CM, the problem is also solved with SolidWorks and Ansys-Workbench programs. SolidWorks program can make three-dimensional designs of structures. In addition, the Simulation module in the SolidWorks program allows different analyses of structural elements. Furthermore, the Ansys-Workbench program has also the capability to perform various analyses on structural elements. In this study, static analysis including large displacements is performed in both programs. In both programs, the uniform model is obtained before analysis. In the study, a three-dimensional solid beam model is used in the SolidWorks program and a one-dimensional line beam model is used in the Ansys-Workbench program for ease of definition. These models are shown in Fig. 15.

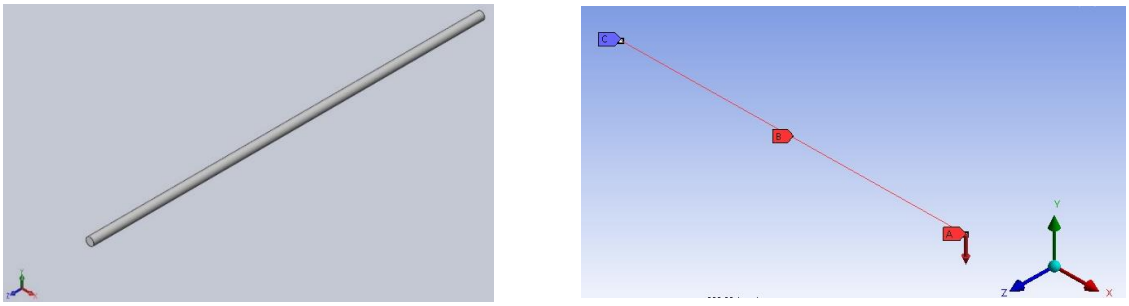


**(a)** Solid beam model in SolidWorks. **(b)** Line beam model in Ansys-Workbench.

**Figure 15.** Beam models.

After the uniform models are obtained in both programs, the material definition process is carried out. For this purpose, special material definition is made in both programs. Eq. 2 is taken as a basis when defining the special material. After the material is defined, the meshing process should be

done. In finite element-based programs, the meshing process needs to be carried out. The meshing process performed in both programs is shown in Fig. 16. As a result of the meshing process, the meshed model has 11707 nodes and 6555 element numbers in the SolidWorks program, and 201 nodes and 100 element numbers in the Ansys-Workbench program.

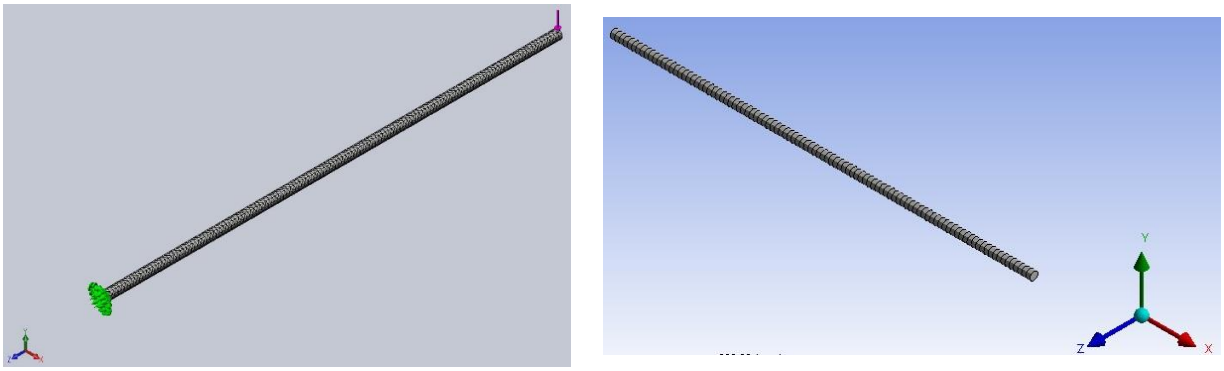

**(a)** Meshed model in SolidWorks. **(b)** Meshed model in Ansys-Workbench.

**Figure 16.** Meshed models.

Clamped boundary condition is applied at one end and a singular load is applied at the other end of the meshed models. The static analysis is then started. The models obtained as a result of the analysis are given in Fig. 17.

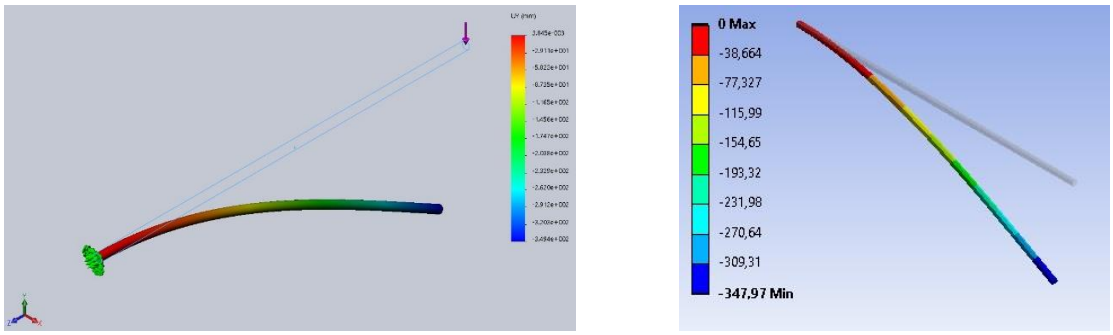


**(a)** The model after analysis in SolidWorks. **(b)** The model after analysis in Ansys-Workbench.

**Figure 17.** The models after analysis.

## 6. RESULT AND DISCUSSION

In this study, a large deflection analysis of a functionally graded beam using the CM is carried out. Moreover, especially, the effects of increasing the force applied to the endpoint of the beam, changing the material index, and changing the beam cross-section on the large deflection of the beam are investigated. Also, the results obtained with CM are compared with the results obtained from SolidWorks and Ansys-Workbench programs for comparison.

### 6.1 Effect of Force

The force applied to the end of the beam is increased to see the effect of the force magnitude on the large deflection of the beam. The force is taken as 100 N, 200 N, 400 N, 800 N, and 1600 N, respectively. Additionally, when examining the force effect, it is assumed that the indexes *n1* and *n2* are taken to be equal to zero. Hence, from Eqs. 1 and 2, *r(s)* and *E(s)* are equal to $r_o$ and $E_o$ respectively. In this study, the radius $r_o$ is constant and equal to 10 mm. As for $E_o$ elasticity modulus,

the material of the beam is assumed to be homogenous, isotropic Aluminum, and its properties are given in Table 1.

**Table 1.** The material properties of Aluminum

| Material | Elasticity Modulus [MPa] | Density [kg/m$^3$] | Poisson's Ratio |
|---|---|---|---|
| Aluminum | 70000 | 2700 | 0.3 |

Fig. 18 shows the behavior of large deflection of the beam under various loads. As can be seen in Fig. 18(a), the beam contains 13 sampling points. The *x* and *y* coordinates of these points are obtained from the CM for the loads mentioned above. Fig. 18(b) shows the large deflection in the *x* and *y* directions of the free end of the beam for given loads.

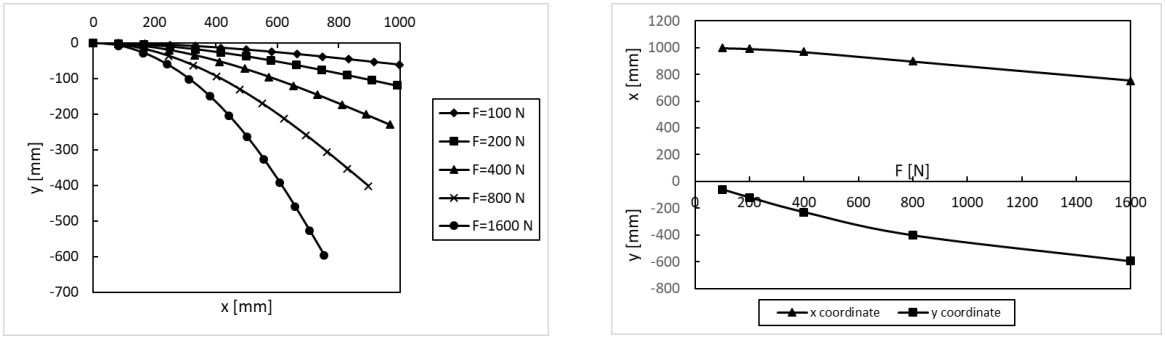


**(a)** Large deflection profiles. **(b)** Coordinates of the free end.

**Figure 18.** The large deflection behavior under various loads.

As shown in the figures, the applied forces are chosen twice the previous one each time. The deflection in the *y* coordinate of the free end of the beam is -60.4025 mm when the force is equal to 100 N, and -595.5787 mm when the force is equal to 1600 N. Therefore, when the force increases by 16 times, the deflection value increases by approximately 9.86 times. As for the variation in the *x* coordinate of the free end of the beam, it is 997.8082 mm when the force is equal to 100 N, and 753.1908 mm when the force is equal to 1600 N. The displacement in the *x* coordinate of the free end of the beam decreases by approximately 1.33 times. In other words, as seen in Fig. 18(b), the position in the y coordinate increases towards to negative direction gradually as the applied force increases. On the other hand, the position in the x coordinate decreases slightly until the force reaches 400N and then decreases rapidly.

### 6.2. Effect of Radius

In order to examine the effect of variation in the cross-sectional area of the beam in the longitudinal direction on large deflection, the radius of the beam is given depending on *s* as seen in Eq. 1. *n1* in this equation is the geometric index, and the variation in beam radius for various values of *n1* is given in Fig. 2. *n1* values are taken as -0.3, -0.15, 0, 0.15, 0.3 in this study. As seen in Fig. 2, when the value of *n1* is equal to zero, the radius of the beam is 10 mm, and the cross-sectional area of the beam is constant. At negative values of the geometric index *n1*, the radius decreases from the clamped end to the free end, and when it is positive, it increases. As for the material index *n2*, it is taken as 0.5. Therefore, the material considered is FGM.

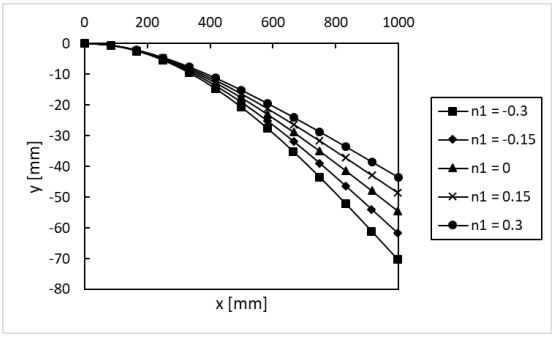


**(a)** Large deflection profiles.

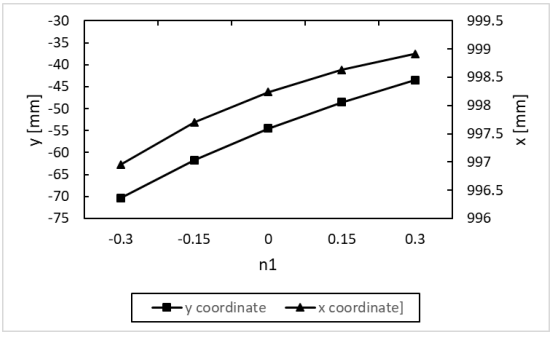


**(b)** Coordinates of the free end.

**Figure 19.** Variation in large deflection with geometric index.

The effect of variation in the geometric index on the large deflection is shown in the two figures above. While examining this effect, it is assumed that the magnitude of the force applied from the free end of the beam is 100 N. When Fig. 19(a) is examined, as expected, the large deflection value increases more as the *n1* value decreases. Because, as the *n1* value decreases, the cross-sectional area of the beam decreases gradually in the longitudinal direction. Fig. 19(b) shows the change of the *x* and *y* coordinates of the free end of the beam with the geometric index *n1*. As can be seen from the figure, the change in both the *x* and *y* coordinates of the free end of the beam increased as the *n1* value decreased.

### 6.3 Effect of Material

As seen in Fig. 3, as the material index (*n2*) changes, the content of the beam material also changes. For positive values of *n2*, the material of the clamped end of the beam becomes *Al*, while the free end is a material with a higher modulus of elasticity than *Al*. When *n2* is equal to zero, the beam material becomes pure *Al*. When *n2* takes a negative value, the clamped end of the beam is again *Al*, but unlike the first case, the free end is a material with a lower modulus of elasticity than *Al*. When examining this effect, *n1* and *F* values are taken as -0.5 and 100 N, respectively. As for *n2* values, they are taken as -0.7, -0.4, 0, 0.4, 0.7.

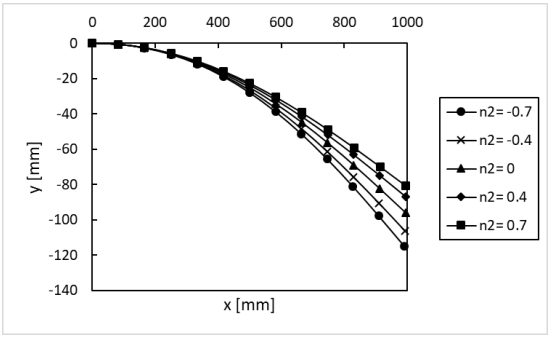


**(a)** Large deflection profiles.

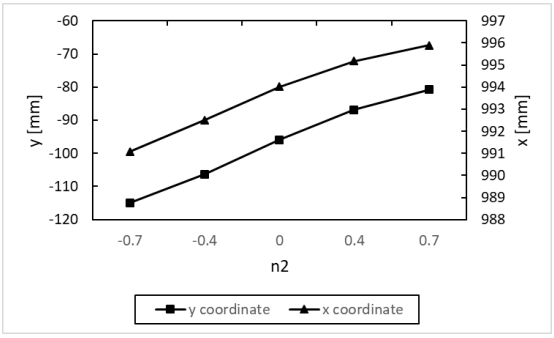


**(b)** Coordinates of the free end.

**Figure 20.** Variations in large deflection with material index.

Fig. 20 shows the effect of the material index on the large deflection behavior of the beam. When Fig. 20 (a) is examined, beams with positive *n2* values deflect less as expected, since the modulus of elasticity directly affects the large deflection of the beam. Fig. 20(b) shows the *x* and *y* coordinates of the deflection of the free end of the beam for different *n2* values. As seen in the figure, the change in both coordinates increases as the *n2* value decreases.

### 6.4 Comparison

In this study, the large deflection behavior of a functionally graded variable cross-section beam is investigated using CM. In order to prove the accuracy of the results obtained with CM, the problem is solved by modeling with SolidWorks-Simulation and Ansys-Workbench programs. Both programs mentioned here are based on the finite element method in their calculations. For comparison purposes, solutions are made in all three methods for different force values by considering a beam of *n1*=0 and *n2*=1. Table 2 shows the comparison of results obtained from CM and Finite Element based programs (FEBP).

**Table 2.** Comparison of results obtained from CM and Finite Element based programs

| Method | Axis | Force [N] | | | | |
|---|---|---|---|---|---|---|
| | | 50 | 100 | 400 | 800 | 1600 |
| Combining Method (CM) | x | 999.64220 | 998.57300 | 978.40620 | 925.78940 | 801.32990 |
| | y | -24.77620 | -49.46500 | -191.32000 | -349.32700 | -550.59300 |
| SolidWorks Simulation | x | 999.29280 | 997.87800 | 975.81000 | 921.50000 | 794.90000 |
| | y | -24.74000 | -49.41000 | -191.30000 | -349.40000 | -552.80000 |
| Ansys Workbench | x | 999.64580 | 998.58720 | 978.61100 | 926.40000 | 802.46000 |
| | y | -24.65300 | -49.22100 | -190.43000 | -347.97000 | -549.2700 |
| % CM-Solid Difference | x | 0.03496 | 0.06962 | 0.26571 | 0.46440 | 0.80563 |
| | y | -0.14603 | -0.11129 | -0.01043 | -0.02086 | -0.40011 |
| % CM-Ansys Difference | x | 0.00036 | 0.00142 | 0.02093 | 0.06593 | 0.14093 |
| | y | -0.49831 | -0.49454 | -0.46625 | -0.38926 | -0.24051 |

The following formula was used when calculating the differences between the results obtained from CM and Finite Element based programs.

$$Percentage\ Difference = 100\ x\ \frac{|\mathrm{FEBP} - \mathrm{CM}|}{\left(\frac{\mathrm{FEBP} + \mathrm{CM}}{2}\right)} \tag{38}$$

When the percentage differences in the table are examined, it is seen that the results obtained with CM are very close to the results obtained with FEBP. When the results are examined, it is seen that the differences in the x coordinate are lower in the one-dimensional finite element analysis, and the differences in the y coordinate are lower in the three-dimensional finite element analysis.

## 7. CONCLUSION

The numerical large deflection solution of a FG beam with variable cross-section is overcome by using CM in this study. Additionally, the problem under consideration is also solved using two finite element-based programs, and a comparison is made. As a result of the numerical analysis, the following results are obtained.

- By increasing the force applied from the free end of a beam with C-F boundary conditions, the y coordinate of the position of the free end of the beam gradually decreases, while the x coordinate decreases slightly until a certain value and decreases rapidly after this value.

- As the cross-section of a beam with C-F boundary conditions decreases from the clamped end to the free end, the large deflection value increases proportionally compared to the constant cross-sectional beam.
- When an FG beam is designed in such a way that the elasticity modulus decreases from the clamped end to the free end, the large deflection amount obtained is greater than the homogenous isotropic beam whose elasticity modulus is not reduced.
- In comparison with the results obtained from finite element-based programs, CM is recommended because it can be easily used in solving geometric nonlinear problems.
- It is seen from the results that the differences in the x coordinate are lower in the one-dimensional finite element analysis, but the differences in the y coordinate are lower in the three-dimensional finite element analysis.
- When the extreme values of the differences between the results obtained from the CM and finite element methods are examined, it is obtained as 0.80563 percent for 1600 N in the x coordinate, while it is -0.49831 percent for 50 N in the y coordinate.

## 8. CONFLICT OF INTEREST

Authors approve that to the best of their knowledge, there is not any conflict of interest or common interest with an institution/organization or a person that may affect the review process of the paper.

## 9. AUTHOR CONTRIBUTION

Ersin DEMİR; Determining the concept and design process of the research, Data Collection, Data analysis and interpretation of the results, Preparation of the manuscript, Critical analysis of the intellectual content, Final approval and full responsibility. Hasan ÇALLIOĞLU; Determining the concept and design process of the research, Data analysis and interpretation of the results, Critical analysis of the intellectual content. Zekeriya GİRGİN; Management of the concept and design process of the research

## 10. REFERENCES

Belendez T., Neipp C., Belendez A., Large and small deflections of a cantilever beam. European Journal of Physics 23, 371-379, 2002.

Brojan M., Cebron M., Kosel F., Large deflections of non-prismatic nonlinearly elastic cantilever beams subjected to non-uniform continuous load and a concentrated load at the free end. Acta Mechanica Sinica 28(3), 863-869, 2012.

Dado M., Al-Sadder S., A new technique for large deflection analysis of non-prismatic cantilever beams. Mechanics Research Communications 32, 692-703, 2005.

Davoodinik A.R., Rahimi G.H., Large deflection of flexible tapered functionally graded beam. Acta Mechanica Sinica 27(5), 767-777, 2011.

Demir E, A numerical study on the large displacement in a functionally graded beam under thermal effect. Journal of Materials and Mechatronics: A 4(2), 492-503, 2023.

Girgin Z., Aysal F.E., Bayrakçeken H., Large deflection analysis of prismatic cantilever beam comparatively by using Combing method and iterative DQM. Journal of Polytechnic 23 (1), 111-120, 2020.

Girgin Z., Combining differential quadrature method with simulation technique to solve non-linear differential equations. International Journal for Numerical Methods in Engineering 75, 722-734, 2008.

Girgin Z., Combining modified integral quadrature method with simulation technique to solve nonlinear initial and boundary value problems. International Journal of Nonlinear Sciences & Numerical Simulation 10(4), 475-482, 2009.

Girgin Z., Yilmaz Y., Demir E., A Combining method for solution of nonlinear boundary value problems. Applied Mathematics and Computation 232, 1037-1045, 2014.

Horibe T., Mori K., Large deflections of tapered cantilever beams made of axially functionally graded material. Bulletin of the JSME Mechanical Engineering Journal 5(1), 1-10, 2018.

Hu Y.J., Liu M., Zhu W., Jiang C., An adaptive differential quadrature element method for large deformation contact problems involving curved beams with a finite number of contact points. International Journal of Solids and Structures 115–116, 200-207, 2017.

Kang Y.A., Li X.F., Large deflections of a non-linear cantilever functionally graded beam. Journal of Reinforced Plastics and Composites 29(12), 1761-1774, 2010.

Kien N.D., Large displacement response of tapered cantilever beams made of axially functionally graded material. Composites Part B 55, 298-305, 2013.

Koizumi M., The concept of FGM. Ceramic Transactions, Functionally Gradient Materials 34, 3-10, 1993.

Kurtaran H., Large displacement static and transient analysis of functionally graded deep curved beams with generalized differential quadrature method. Composite Structures 131, 821-831, 2015.

Li Z., Huang D., Yan K., Xu Y., Large deformation analysis of functionally graded beam with variable cross-section by using peridynamic differential operator. Composite Structures 279, 1-13, 2022.

Lin X., Huang Y., Zhao Y., Wang, T., Large deformation analysis of a cantilever beam made of axially functionally graded material by homotopy analysis method. Applied Mathematics and Mechanics (English Edition) 40(10), 1375-1386, 2019.

Nguyen D.K., Bui T.T.H., Tran T.T.H., Alexandrov, S., Large deflections of functionally graded sandwich beams with influence of homogenization schemes. Archive of Applied Mechanics 92, 1757-1775, 2022a.

Nguyen V.X., Nguyen K.T., Thai S., Large deflection analysis of functionally graded beams based on geometrically exact three-dimensional beam theory and isogeometric analysis. International Journal of Non-Linear Mechanics 146, 1-16, 2022b.

Saraçoğlu M.H., Güçlü G., Uslu F., Deflection analysis of functionally graded equal strength beams. European Mechanical Science 6(2), 119 - 128, 2022.

Saraçoğlu M.H., Güçlü G., Uslu F., Static Analysis of Orthotropic Euler-Bernoulli and Timoshenko Beams with Respect to Various Parameters 8(2), 628 - 641, 2019.

Sitar M., Kosel F., Brojan M., Large deflections of nonlinearly elastic functionally graded composite beams. Archives of Civil and Mechanical Engineering 14, 700-709, 2014.

Soleimani A., Large deflection of various functionally graded beam using Shooting Method. Applied Mechanics and Materials 110-116, 4705-4711, 2012.